Acta Crystallographica Section D
Biological Crystallography
ISSN 0907-4449

Refinement of the arginine kinase transition-state analogue complex at 1.2 Å resolution: mechanistic insights

Mohammad S. Yousef,[a]†‡ Felcy Fabiola,[a]† James L. Gattis,[b] Thayumanasamy Somasundaram[a] and Michael S. Chapman[a,b]*

[a]Institute of Molecular Biophysics, Florida State University, Tallahassee, FL 32306-4380, USA, and [b]Department of Chemistry and Biochemistry, Florida State University, Tallahassee, FL 32306-4380, USA

† These authors contributed equally to this work.
‡ On leave of absence from the Biophysics Department, Faculty of Science, Cairo University, Egypt.

Correspondence e-mail: chapman@sb.fsu.edu

Received 10 April 2002
Accepted 12 August 2002

PDB Reference: AK-TSAC, 1m15, r1m15sf.

The three-dimensional crystal structure of an arginine kinase transition-state analogue complex has been refined at 1.2 Å resolution, with an overall R factor of 12.3%. The current model provides a unique opportunity to analyze the structure of a bimolecular (phosphagen kinase) enzyme in its transition state. This atomic resolution structure confirms in-line transfer of the phosphoryl group and the catalytic importance of the precise alignment of the substrates. The structure is consistent with a concerted proton transfer that has been proposed for an unrelated kinase. Refinement of anisotropic temperature factors and translation–libration–screw (TLS) analyses led to the identification of four rigid groups and their prevalent modes of motion in the transition state. The relative magnitudes of the mobility of rigid groups are consistent with their proposed roles in catalysis.

1. Introduction

Arginine kinase (AK) is an invertebrate homalogue of mammalian creatine kinase (CK); both enzymes belong to the phosphagen kinase family. These enzymes play an important role in cells by buffering ATP concentration depending on cellular energy requirements (Ellington, 2001; Schlattner *et al.*, 1998). Phosphagen kinases catalyze the reversible transfer of a phosphoryl group between ATP and a phosphagen, in this case arginine phosphate:

$$\text{arginine} + \text{MgATP} \longleftrightarrow \text{arginine phosphate} + \text{MgADP}.$$

Although phosphagen substrates are quite different, AK and CK are thought to share a common mechanism of associative in-line γ-phosphoryl transfer (Hansen & Knowles, 1981). Several phosphagen kinase structures have been solved at different resolutions: firstly chicken sarcomeric mitochondrial CK (Mt-CK_{sar}) at ~3 Å with and without ATP (Fritz-Wolf *et al.*, 1996) and AK from the horseshoe crab *Limulus polyphemus* as a transition-state analogue complex (TSAC) at 1.86 Å (Zhou *et al.*, 1998), then the following, all as substrate-free enzymes: rabbit muscle CK (M-CK) at 2.35 Å (Rao *et al.*, 1998), chicken cytosolic brain-type CK at 1.4 Å (Eder *et al.*, 1999), human ubiquitous mitochondrial CK (Mt-CK_{ubi}) at 2.7 Å (Eder *et al.*, 2000), cytosolic bovine retinal CK at 2.3 Å (Tisi *et al.*, 2001) and human M-CK at 3.5 Å (Shen *et al.*, 2001). Owing to substrate-induced conformational changes (Zhou *et al.*, 2000), it is only AK-TSAC that gives clear structural evidence of the catalytic mechanism. ADP and arginine are bound in a dead-end complex with nitrate mimicking a trigonal phosphoryl group during in-line transfer (Hansen & Knowles, 1981; McLaughlin & Cohn, 1972; Milner-White & Watts, 1971).

Protein structures at atomic resolution are relatively rare. However, recent advances have resulted in an improved ability to obtain atomic resolution diffraction from protein crystals and to subsequently determine structures at atomic and subatomic resolution (Dauter *et al.*, 1997; Longhi *et al.*, 1998). Atomic resolution data, by Sheldrick's criteria, extend to 1.2 Å or better with at least 50% of the diffraction intensities of the outer resolution shell above 2σ (Sheldrick, 1990). With data to 1.2 Å or better, it is possible to refine parameters that describe not only the overall motion of model atoms, but which directions of motion are preferred. Higher resolution X-ray data for arginine kinase have enabled us to refine individual atomic displacement parameters anisotropically. The preferred direction of atomic displacements can be rationalized in terms of the enzyme mechanism.

The translation–libration–screw (TLS) method provides an alternative formalism to represent molecular motions by constrained rigid groups of atoms. Schomaker & Trueblood (1968) showed that the anisotropic displacements of rigid groups of atoms could be described by three tensors: translation (T), libration (torsional vibration) (L) and screw-rotation (S). TLS refinement involves far fewer parameters (six from T, six from L and eight from S for each rigid group) compared with the refinement of individual atomic displacement parameters. It has been used for several macromolecular refinements (Holbrook & Kim, 1984; Holbrook *et al.*, 1985; Howlin *et al.*, 1989; Sali *et al.*, 1992; Papiz & Prince, 1996). TLS refinement requires the prior designation of rigid groups of atoms and the results may be sensitive to this choice. However, methods are now available for the fitting of TLS parameters to the refined individual anisotropic displacement parameters (Stec *et al.*, 1995; Harata *et al.*, 1998, 1999; Wilson & Brunger, 2000). Thus, the designation of rigid groups can be cross-validated in studies at high enough resolution for both TLS and individual anisotropic displacement parameters refinements.

A survey of literature and the Protein Data Bank indicates that arginine kinase, at 42 kDa, is among the largest protein structures refined at atomic resolution (Teixeira *et al.*, 2001). It is also the only high-resolution structure of a bimolecular enzyme as a transition-state analogue in which the components are bound independently (and not covalently joined in a bisubstrate complex) in an active site that has not been mutated to slow or stop the reaction. Thus, this offers a unique opportunity to examine the role of unperturbed substrate alignment in the enzyme catalysis of multi-substrate reactions, complementing earlier studies of substrate–cofactor interactions (Mesecar *et al.*, 1997).

Detailed studies of a bimolecular transition-state complex were motivated by unresolved issues of how the catalysis of multi-substrate reactions may differ fundamentally from the unimolecular systems (proteases, glycosidases, nucleases *etc.*) that have been studied more extensively. It is widely recognized that part of the catalytic effect may be achieved by pre-aligning the reactants on favorable reaction trajectories. However, there is little consensus as to its importance among the various means of enhancing rate (Warshel, 1998; Bruice & Benkovic, 2000; Lau *et al.*, 2000; Villa *et al.*, 2000). Some of the contention has arisen from a narrow focus on entropic terms, but calculations on unimolecular and bimolecular systems indicate that the adoption of near-attack conformers is accompanied by larger enthalpic changes than entropic (Lightstone & Bruice, 1996, 1998). Thus, there are compelling reasons to understand substrate pre-alignment whenever it is possible to observe it directly.

The 1.86 Å resolution structure of the transition-state analogue showed that the active site positioned the reactants along the optimal reaction trajectory, at least approximately (Zhou *et al.*, 1998). Understanding the precision of alignment presented a crystallographic challenge, because the parameters of interest were unrestrained non-bonded distances and angles between substrate molecules. Thus, the crystallographic challenge of the refinement of a 42 kDa enzyme at 1.2 Å resolution was undertaken.

Table 1
Data-processing statistics.

Outer-shell values are shown in parentheses.

Resolution range (Å)	20–1.2 (1.23–1.20)
No. of observations	1112071
No. of unique reflections	115910
Completeness (%)	96.2 (71.5)
$R_{\rm sym}$ (%)	4.8 (32.3)
$I/\sigma(I)$	24 (2.1)
Unit-cell parameters (Å)	a = 65.393, b = 70.312, c = 80.139
Space group	$P2_12_12_1$

2. Materials and methods

2.1. Data collection and processing

AK from horseshoe crab was expressed, purified and complexed with analogue components (ADP, nitrate and arginine) as previously described (Zhou *et al.*, 1997). AK-TSAC crystals were then obtained at pH 7.5 by equilibrating against 15–20% PEG 6000 using previously reported crystallization conditions (Zhou *et al.*, 1997). Cryocrystallographic data on several crystals were collected on beamline X12-B (λ = 0.95 Å) at the National Synchrotron Light Source at Brookhaven National Laboratory. The final data set was collected by flash-cooling one crystal (0.4 × 0.5 mm) in a nitrogen stream maintained at 100 K. Data were collected with an oscillation width of 0.5° using a Quantum 4 CCD detector (ADSC, Poway, California, USA), a sample-to-detector distance of 100 mm and exposures of 60 s. Integration and scaling of the synchrotron data set was performed using the *HKL* suite of programs, *DENZO*, *XDISPLAYF* and *SCALEPACK* (Otwinowski & Minor, 1997). Table 1 shows the statistics of the data processing.

2.2. Structure refinement

The 1.86 Å AK-TSAC structure (Zhou *et al.*, 1998) was used as the starting model for refinement. The same reference set of 3% of the reflections used in the calculation of $R_{\rm free}$ (Brünger, 1992) was extended to include 1.86–1.2 Å data. A working set

of the remaining 97% of the reflections was used throughout *CNS* and *SHELXL*97 refinement using data in the resolution range 6.0–1.2 Å (low-resolution terms were truncated for improved scaling).

Rigid-body refinement using *CNS* (Brünger *et al.*, 1998) and with fixed thermal factors of 15 Å^2 improved the model from R and R_{free} of 27.9 and 28.2% to 27.5 and 28.1%, respectively. Several rounds of positional refinement by simulated annealing, along with B-factor refinement, water picking and manual rebuilding of the model reduced R and R_{free} to 16.1 and 17.49%, respectively (Fig. 1). Further refinement used *SHELXL*97 (Sheldrick & Schneider, 1997). Ten cycles of conjugate-gradient least-squares refinement with individual isotropic thermal factors led to no improvement. Progress was made with conjugate-gradient anisotropic refinement using six-parameter anisotropic displacement parameters with restraints for bond lengths, angles, planarity, chirality and anti-bumping. There was dramatic improvement in R and R_{free} to 11.7 and 14.7%, respectively, demonstrating that the anisotropic refinement was meaningful. The model improved to R and R_{free} of 11.6 and 12.9%, respectively, with the addition of a further 60 water molecules using the automated water-searching program *SHELXWAT* (Sheldrick & Schneider, 1997). New atoms were always refined isotropically before making them anisotropic.

Riding H atoms were generated using *SHELXL* on the basis of the expected stereochemistry. Although hydrogen positions could not be discerned directly from the difference map, the addition of H atoms to the model resulted in significant improvement (R and R_{free} = 11.0 and 12.3%, respectively). The hydrogen coordinates were not refined explicitly, but implicitly based on the positions of bonded heavier atoms. Final refinement used all the data including test reflections previously set aside for cross-validation. This refinement converged to an R factor of 10.7% for 42 267 reflections with $F_o > 4\sigma(F_o)$ and 12.3% for all 105 688 reflections ($F_o > 0$) in the range 6–1.2 Å. Fig. 1 shows the progress of refinement and Tables 2 and 3 show the relevant statistics.

2.3. Final model

After each of the refinement rounds, the model was inspected manually using ($2F_o - F_c$) Fourier maps visualized in the program *O* (Jones *et al.*, 1991). During rebuilding, all electron-density peaks greater than 5σ in a ($F_o - F_c$) map were checked for indications that coordinates, B factors or occupancies needed to be changed. At the end of refinement, the ($F_o - F_c$) map was essentially featureless.

The backbone is well ordered and multiple conformations are restricted to some disordered side chains. Two alternate rotamers were modelled for residues Lys28, Met46, Lys102, Lys151, Arg312 and Ser318. (The most striking case is Ser154, where three conformations were clearly visible in the electron density.) In addition to the transition-state analogue components, the final model contains a second bound nitrate, far from the active site and of no biochemical significance. The details of the final model are provided in Table 2.

In order to estimate the error in the final model, a final cycle of blocked full-matrix least-squares refinement (FMLS) was

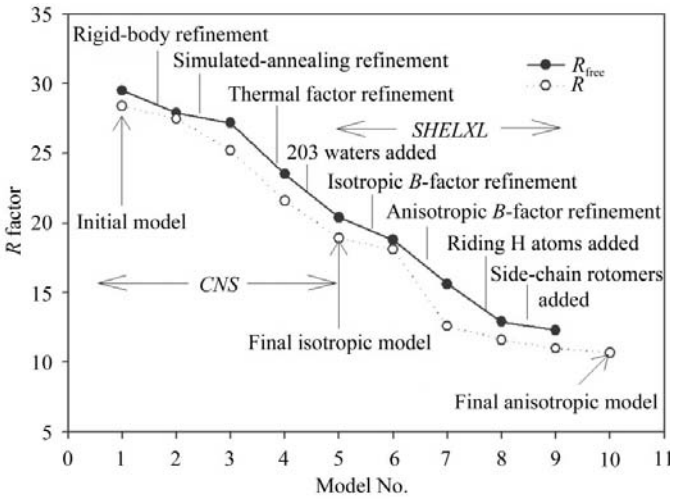

Figure 1
Progress of refinement. R and R_{free} calculations are based on 2σ and 4σ cutoffs for *CNS* and *SHELXL*, respectively.

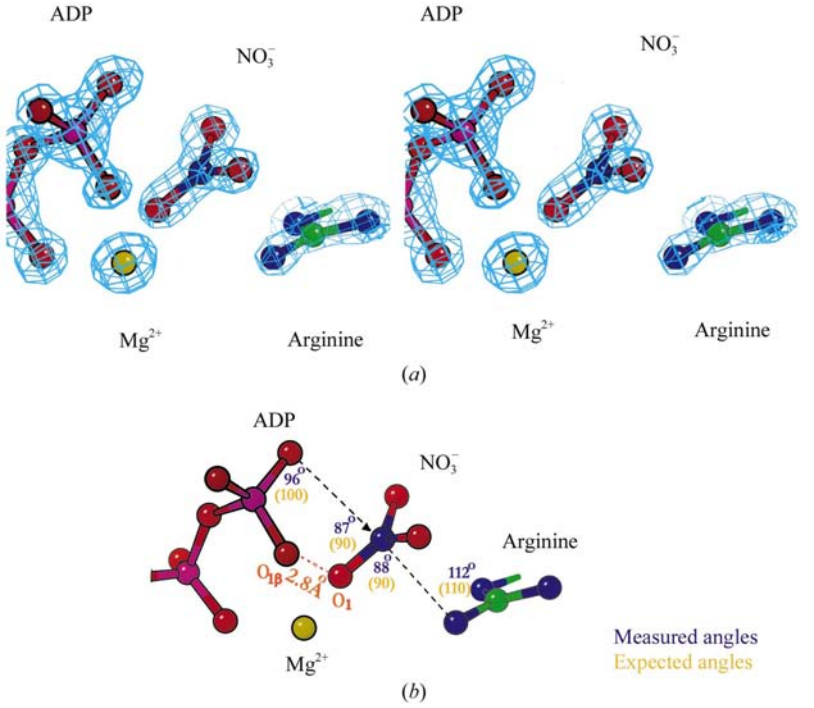

Figure 2
(*a*) Precise alignment of the substrates in the active site as revealed by the $2F_o - F_c$ electron-density map contoured at 3σ. (*b*) The in-line transfer of the phosphoryl group and the hydrogen-bond geometry between $O_{\beta 1}$ of ADP and O_1 of nitrate. Angles in parentheses correspond to the optimal reaction trajectory (Zhou *et al.*, 1998).

Table 2
Final refinement statistics.

Refinement programs	*CNS*, *SHELXL*
Resolution in final refinement (Å)	6–1.2
No. of reflections	102470
R factor including all data ($I > 0\sigma$) (%)	12.25
R/R_{free} ($I > 4\sigma$) (%)	10.82/12.25
No. of protein atoms	2866
No. of water molecules	557
No. of other molecules	1 arginine, 2 NO_3, 1 ADP, 1 Mg^{+2}
No. of alternate conformations	7 amino acids
Mean *B* factors (Å^2)	
All atoms	16.7
Protein	16.8
Main chain	14.8
Side chain	17.5
Water molecules	35
Substrates	10
R.m.s. deviation from ideal geometry	
Bond length (Å) (with/without restraints)	0.013/0.089
Bond angle (°) (with/without restraints)	1.33/2.61
Luzzati coordinate error† (Å)	0.04
Ramachandran plot‡	
Residues in most favoured region (%)	92.3
Residues in additional allowed region (%)	7.1
Residues in generously allowed region (%)	0.6
Residues in disallowed region	0.0

† Luzzati (1952). ‡ Ramakrishnan & Ramachandran (1965).

Table 3
Crystallographic *R* (for all data) and R_{free} (for all data) as a function of resolution.

Resolution range (Å)	R_{free}	*R*
100–4.8	28.4	21.0
4.8–3.4	13.9	13.4
3.4–2.8	12.5	11.9
2.8–2.4	12.7	10.9
2.4–2.1	12.1	10.4
2.1–2.0	12.1	10.7
2.0–1.8	11.3	10.3
1.8–1.7	11.9	10.6
1.7–1.6	14.1	10.7
1.6–1.5	14.3	11.9
1.5–1.45	14.4	12.6
1.45–1.39	14.6	13.9
1.39–1.33	16.4	15.5
1.33–1.28	17.8	17.1
1.28–1.24	21.2	19.3
1.24–1.20	21.8	21.4

performed with no restraints, which provided a more reliable estimate of coordinate errors. The protein was divided into 30 blocks of 15 residues, each with a one-residue overlap. The final values of the standard deviation parameters were 0.089 Å for bond lengths and 2.61° for bond angles for the unrestrained model. These values are substantially higher than those obtained after imposition of stereochemical restraints (0.013 Å for bond lengths, 1.33° for bond angles for the restrained model); however, unrestrained bond lengths and angles have the advantage of being dependent only on the experimental X-ray data and therefore not biased by target values; the unrestrained model was not used for any further refinement.

A Luzzati plot (Luzzati, 1952) was used to estimate the accuracy of atomic positions (0.04 Å). *PROCHECK* was used to perform the geometric analysis of the final model (Laskowski *et al.*, 1993). A Ramachandran plot (Ramakrishnan & Ramachandran, 1965) of the observed values of conformational angles for the model shows no residues in the disallowed region. The program *PARVATI* (Merritt, 1999) was used to analyse the final distribution of *B*-factor anisotropy among the protein and solvent.

2.4. Molecular-mechanics calculation

Molecular-mechanics calculations were performed using the *DISCOVER* program with the AMBER force field (Biosym Technologies). The close proximity (2.8 Å) between the nitrate O_1 and the ADP phosphate $O_{1\beta}$ led us to consider protonation of one or the other, hydrogen bonding between them and possible proton transfer associated with phosphoryl transfer. ADP protonation states were determined by p*K* calculations with the finite difference Poisson Boltzman method using *Delphi* (Yang *et al.*, 1993) and also with molecular-mechanics calculations. The molecular-mechanics calculations were used to assess the consistency of several possible protonation states with the experimentally determined atomic coordinates: (i) a negative unit charge assigned to the ADP $O_{1\beta}$ and to the nitrate O_1 in the presence of Mg^{2+}; (ii) a hydrogen fixed on $O_{1\beta}$ and a negative unit charge assigned to the nitrate O_1; (ii) a partial charge of −0.33 assigned to each of the three O atoms of the nitrate and a negative unit charge to the ADP $O_{1\beta}$.

2.5. TLS refinement

In order to assess the rigidity of the protein, the structure was divided into different rigid groups and TLS refinements were performed. The selection of the rigid groups was based on the Rosenfield *et al.* (1978) rigid-body postulate, where the possible quasi-rigid groups in a protein are identified from low Δ values. The postulate is based on the assumption that as the interatomic distances within a rigid body are fixed, the difference in the projections of the anisotropic displacement parameters of two atoms in a rigid body (the 'Δ' value) must be zero. This applies to all pairs of atoms in a rigid body and not just bonded pairs. Since proteins are never completely rigid, possible quasi-rigid groups are identified from low values of Δ for the group of atoms. Δ-matrix analysis showed four rigid groups within the protein (see Fig. 5).

To validate the rigid-body designation from the Δ-matrix analysis, alternate rigid-group assignments were tested as follows.

(*a*) The entire protein.

(*b*) Two groups: (i) residues 2–99 (small domain) and (ii) residues 100–357 (large domain).

(*c*) Three groups: (i) residues 2–99 (small domain); (ii) residues 100–308 and 320–357 and (iii) residues 309–318 (loop 1).

(*d*) Four groups: (i) residues 2–99 (small domain), (ii) residues 100–280 (large domain), (iii) residues 281–308 (loop 2) and (iv) residues 309–357 (terminal domain).

The 1.86 Å structure was the basis for the selection of cases (*b*) and (*c*), as it was shown that AK consists of a small domain (residues 2–99), a large domain (100–357) and a catalytic loop (309–318) within the large domain (Zhou *et al.*, 1998). The selection of case (*d*) was based on the Δ-matrix analysis. In every case, the temperature-factor profile obtained from the refined individual anisotropic displacement parameters (represented by their isotropic equivalent U_{iso}) was compared with that calculated from the TLS refinement.

TLS refinement was performed using the program *RESTRAIN* (Collaborative Computational Project, Number 4, 1994) and TLS tensors were determined by the least-squares method using C^{α} atoms. The resulting TLS tensors were analyzed using the program *TLSANL*; the program *ANISOANL* (Collaborative Computational Project, Number 4, 1994) was used to produce temperature-factor plots.

3. Results and discussion

3.1. Enzyme mechanism

3.1.1. In-line transfer of the phosphoryl group and precise alignment of the substrates. The high quality of the electron-density map allows precise modeling of the active site and substrates (Fig. 2*a*). With the non-reactive nitrate mimicking the analogous phosphoryl of the transition state, it is clear that substrates are positioned near optimally for the in-line transfer of the phosphoryl group (Fig. 2*b*). The donor and the acceptor atoms (ADP-$O_{3\beta}$ and guanidyl $N_{\eta 2}$ of substrate arginine) are positioned to form bonds almost orthogonal to the nitrate plane, just 3 and 2° from ideal, respectively. Regarding the nucleophilic attack by the guanidyl $N_{\eta 2}$, the optimal angle for the attacking lone pair is ∼110° to the $N_{\eta 2}-C_{\gamma}$ bond in a plane perpendicular to the guanidine plane (Zhou *et al.*, 1998). The $C_{\gamma}-N_{\eta 2}-N$ approach angle between arginine and nitrate (mimicking P_{γ}) is ∼112°, 2° from ideal. For the reverse reaction, extended Hückel calculation of phosphate valence electron density suggests that the optimal angle for nucleophilic attack by ADP-$O_{3\beta}$ is 100° (Zhou *et al.*, 1998) with respect to the P_{β}–$O_{3\beta}$ bond. The observed P_{β}–$O_{3\beta}$–N (P_{γ}) angle is ∼96°, 4° from optimal. The r.m.s. deviation from ideal trajectories of the four angles of approach is 2.9°, which is little more than the 2.6° estimated error in unrestrained angles. This precision of alignment is similar to that envisioned in Koshland's orbital steering (Dafforn & Koshland, 1971), even though the calculations have been called into question by Jencks (Page & Jencks, 1971). The alignment is more precise than required by Jenck's estimation of the impact of entropy on reaction rate. At this stage, it is not possible to differentiate between several possibilities: (i) whether the precise alignment is purely accidental, (ii) whether the enzyme has evolved to exploit even marginal improvements in rate achievable with very precise alignment or (iii) whether the catalytic effect of precise alignment is underestimated by the approximations of current theory.

Notable also is the lack of disorder in the substrates. Not being part of the polypeptide chain, one might expect the motion of the substrates to be less restrained. However, the mean isotropic *B* factor for substrates (10 $Å^2$) is lower than for protein (17 $Å^2$) and the same as internal amino acids. Thus, the active site is not only pre-aligning them, but also constraining their motional freedom, reducing the entropy of activation.

It is noteworthy to mention that, although there are no covalent bonds to constrain them, the positions and geometry of the substrate-analogue components are remarkably consistent with the presumptive transition state in which a trigonal phosphoryl group is partially covalently bound midway between the ADP and arginine acceptor/leaving groups (Hansen & Knowles, 1981; McLaughlin & Cohn, 1972; Milner-White & Watts, 1971). For example, the observed distance between guanidino N and O_{β} through the analogue nitrate is 6 Å, which is identical to that which is expected of the transition state (Hansen & Knowles, 1981). Furthermore, the position of the nitrate of the analogue is not constrained by (partial) covalent bonding to the β-phosphoryl or guanidinium, yet is positioned nearly exactly where the γ-phosphoryl would be expected (Figs. 2*a* and 2*b*) in the transition state. These observations, along with the angles of approach discussed previously, confirm that this dead-end inhibitory complex mimics the actual transition-state complex very well.

3.1.2. Concerted proton transfer. The distance of 2.8 Å between ADP $O_{1\beta}$ and O_1 of nitrate indicates a likely hydrogen bond (Fig. 2*b*). Molecular-mechanics calculation showed that the distance would be 3.2 Å without a shared proton. With different hypothetical charge/protonation states, we obtained a close approximation to the X-ray geometry only when $O_{1\beta}$ of ADP was uncharged (*i.e.* either protonated or double bonded) and a unit negative charge was assigned to the

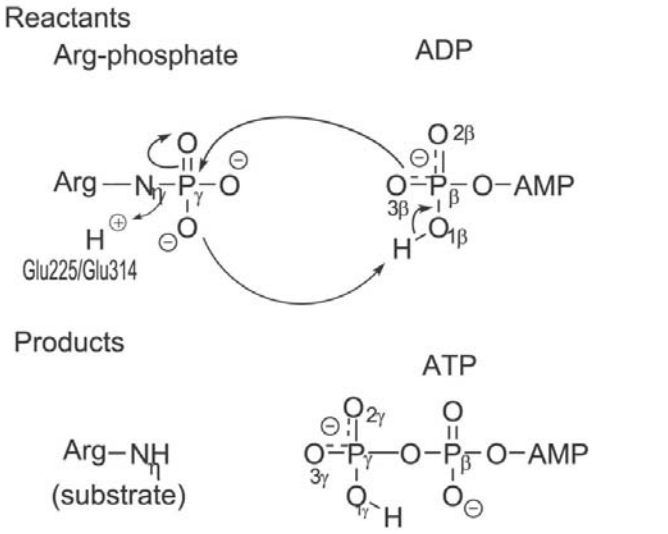

Figure 3
The proposed proton-transfer mechanism for the half-reaction. Arrows indicate the motion of electrons. Arginine is initially phosphorylated at the guanidino nitrogen N_{η}.

O_1 of the nitrate. pK_a values of the ADP β O atoms, calculated by the finite difference Poisson Boltzman method (Yang *et al.*, 1993), show that the $O_{2\beta}$ is double bonded and that $O_{1\beta}$ and $O_{3\beta}$ are mostly protonated when bound in the active site. These calculations are consistent with ^{31}P NMR data that show that the pK_a value of the β-phosphate of MgADP increases from 6 (in solution) to 7.5 upon binding to arginine kinase in a TSA complex (Rao & Cohen, 1977). These various arguments point to the $O_{1\beta}$ being predominantly protonated under physiological conditions. This can be rationalized by the proximity of negative charges in its environment. $O_{1\beta}$ is $\sim$2.8 Å from both the ADP $O_{1\alpha}$ and the nitrate O_1. There may be minor differences between the TSA complex and the real transition state. Nitrate has a lower pK than ADP, so a shared proton would be located predominantly on the β-phosphate (Izzat & Christensen James, 1970). In the actual transition state, it might be more equally shared, but present nonetheless, leading us to propose a concerted proton transfer synchronized with the phosphoryl transfer (Fig. 3).

The proposed concerted proton transfer follows other precedents in phosphoryl-transfer reactions. A similar proposal resulted from quantum-mechanical calculations for the reaction of cyclic 3′,5′-adenosine monophosphate (cAMP) dependent protein kinase (Hutter & Helms, 1999) and for UMP/CMP kinase (Hutter & Helms, 2000). The calculations showed that in both systems phosphoryl transfer is accompanied by simultaneous transfer of a proton.

For arginine kinase, the implications of the proton transfer would be that loss of the $O_{1\beta}$ proton would lead to electron migration towards P_β. Excess negative charge on P_β would facilitate the migration of the $O_{3\beta}$ electron, thus enhancing nucleophilic attack during the formation of the new bond with P_γ. Upon bond formation, excess charge on P_γ (N in our substrate analogue) would lead to electron migration towards the $O_{1\gamma}$ of the phosphoryl (O_1 of nitrate in the analogue), favouring acceptance of the $O_{1\beta}$ proton. The cycle is complete. It is, of course, impossible to distinguish cause and effect, because the whole process would be concerted.

3.1.3. Mg^{2+} ion. The preferred coordination number of Mg^{2+} is six and magnesium has a strong preference to bind to O atoms as electron donors (Katz *et al.*, 1996). Crystallographic database analysis on small-molecule structures showed that the metal–oxygen distances lie in the range 2.00–2.15 Å, with a mean of 2.07 Å (Harding, 1999). In the current crystal structure, the metal–oxygen distances range from 2.01–2.15 Å (mean of 2.07 Å) and form an octahedral coordination sphere around the metal.

The high-resolution structure shows that Mg^{2+} in the active site has two coordination spheres (Fig. 4): the first sphere is of radius $\sim$2 Å, consisting of $O_{1\alpha}$, $O_{1\beta}$ of ADP, O_1 of the nitrate and three water molecules as coordinating elements. The second sphere is of radius $\sim$4 Å, consisting of Glu224, Glu225 and Glu314. The distance between the carboxyl O atom of these residues and Mg^{2+} are 4.2, 4.4 and 4.1 Å, respectively. These negatively charged residues interact indirectly with Mg^{2+} *via* hydrogen bonds bridged by three Mg^{2+}-liganding water molecules. Glu314 and Glu225 are catalytically important residues, holding the substrate arginine in place and perhaps acting upon it, in an acid–base catalytic role (Zhou *et al.*, 1998).

The coordination of Mg^{2+} plays an important role in the catalysis at several levels. If it is removed from molecular-mechanics models, the distance between phosphate $O_{1\beta}$ and nitrate O_1 increases from 2.8 to 4.7 Å. Thus, the Mg^{2+} allows close approach of the γ-phosphoryl and β-phosphate groups. Secondly, the Mg^{2+} is essential in configuring the active site. The catalytic Glu314 that is in the second coordination sphere

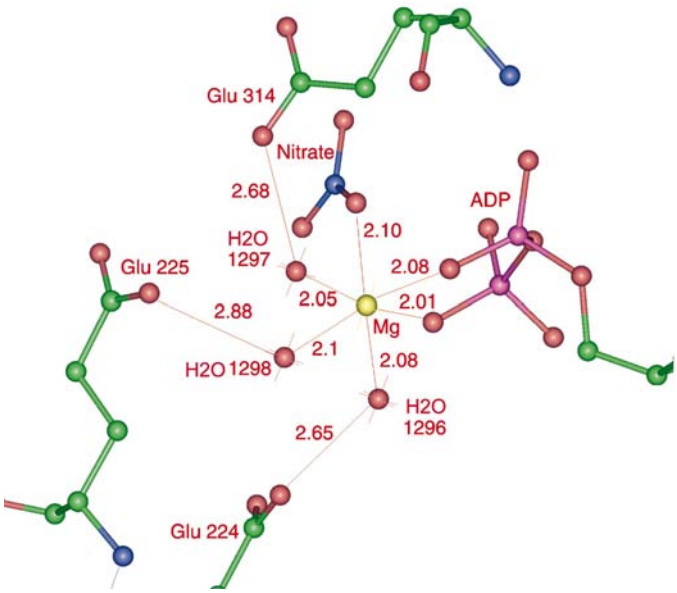

Figure 4
Coordination of Mg^{2+} in the active site. Distances are shown in Å.

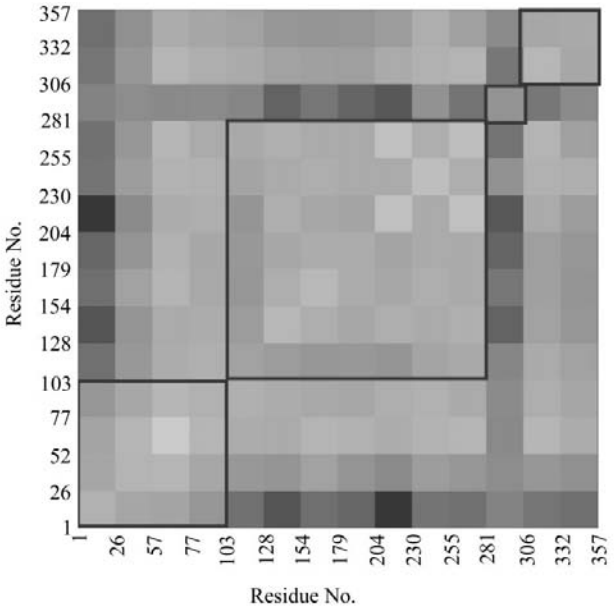

Figure 5
The Δ matrix. Shading corresponds to the Δ values. Blocks of uniformly light shading indicate possible rigid bodies. This figure was produced with the program *ANISOANAL* (Collaborative Computational Project, Number 4, 1994).

is within a loop that is disordered and folded away from the active site in substrate-free structures of creatine kinase (Fritz-Wolf *et al.*, 1996). The role of the Mg^{2+} in stabilizing the new position of Glu314 in the substrate-bound closed enzyme structure may explain the solution-scattering observations that binding of ADP or ATP with Mg^{2+} elicits a large conformational change, but not the free nucleotide without Mg^{2+} or the guanidine substrate (Forstner *et al.*, 1998).

3.2. Analysis of thermal motion

The high-resolution data allows the variation in each position to be described by six anisotropic displacement parameters. The mean anisotropy (related to the lengths of the shortest and longest principal axis of the corresponding ellipsoid) is 0.42 for the protein, with a standard deviation of 0.12. This means that the ellipsoids approximating the thermal motion of atoms are twice as large in one direction as the other. This is typical of the values found in an earlier survey of other proteins (Merritt, 1999). Also, atoms near the center of the molecule have rather isotropic displacements, but regions that are exposed to the solvent region exhibit greater anisotropic motion.

Δ-matrix analysis (Fig. 5) indicated four rigid groups. The designation of the exact boundaries of different groups was adjusted based on our prior knowledge of the structure (Zhou *et al.*, 1998). The designated rigid groups are: (i) residues 2–99 (small domain), (ii) residues 100–280 (large domain), (iii) residues 281–308 (loop 2) and (iv) residues 309–357 (terminal domain). Comparison of the isotropic equivalent displacement factors calculated from the TLS and ADP refinements confirmed that the rigid-body designations from Δ-matrix analysis were reasonable, as the correlation was much improved compared with when the protein was considered as a single rigid body (Fig. 6*a*). Two and three rigid-group models were insufficient to obtain good agreement between TLS and anisotropic displacement parameter refinement, especially for loop regions (Figs. 6*b* and 6*c*). The best fit was obtained only with the four-rigid-group TLS model (Fig. 6*d*).

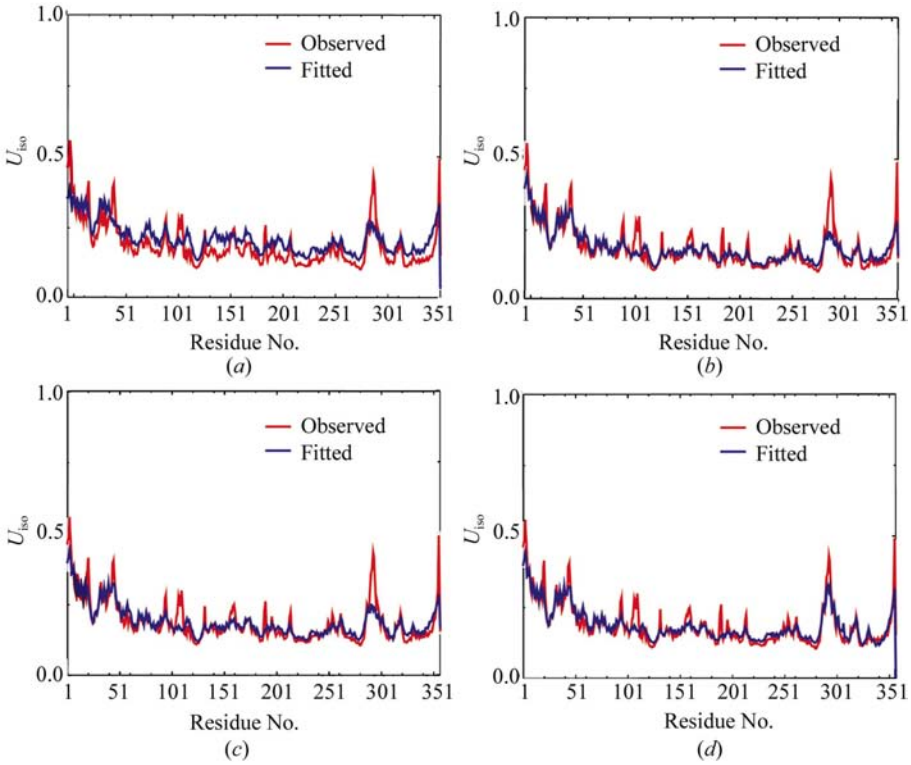

Figure 6
Comparison of isotropic equivalent atomic displacement factors (U_{iso}) supports the four-rigid-group model. U_{iso} calculated directly from the TLS refinement is plotted in blue and U_{iso} from the individual anisotropic displacement parameters of *SHELXL* refinement is in red. (*a*) A TLS model in which the entire protein has been considered as a rigid group; (*b*) a TLS model with two rigid groups; (*c*) a TLS model with three rigid groups; (*d*) the TLS model with four rigid groups as indicated by the Δ analysis. See §2.5.

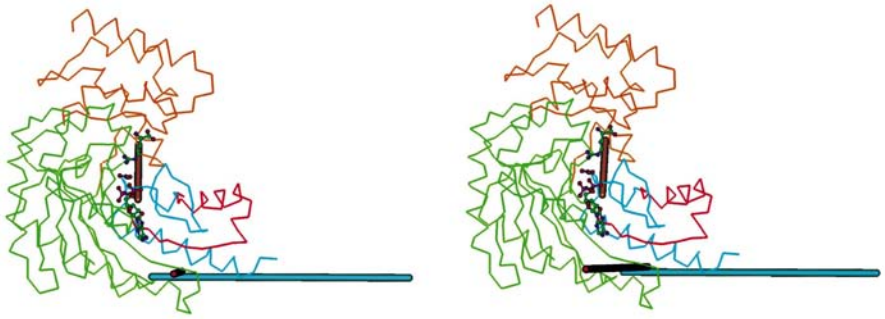

Figure 7
Stereoview of the segmented domain TLS model. The librational tensors are shown in colors that correspond to the coloring of the domains in the C_α trace: orange, small domain (2–99); cyan,C-terminal domain (309–357); red, loop (281–308). The length of the axes is proportional to the magnitude of libration. Although the length of the red axis appears to show that the libration of the loop is small, it is in fact the largest but looks smaller because the direction of view is almost directly down the axis. There is no prevalent motion associated with the large (green) domain (100–280). The substrates are shown in ball-and-stick representation.

The direction and magnitude of librational components of the TLS model with four rigid groups are given in Table 4. The principal axes of the libration tensors are shown in Fig. 7. Unlike libration, the translational and screw tensors have eigenvalues that are approximately equal in all the directions for the different rigid groups (data not shown), indicating the translational and screw disorder was largely isotropic. The librational motion of the large domain (100–280) is also small

Table 4
Eigenvectors and eigenvalues of libration tensors for the protein rigid groups in the TLS refinement.

The protein is split into four rigid groups (L1–L4; see text).

	Eigenvector			Eigenvalue
L1	0.354	−0.908	0.225	0.789
	0.881	0.405	0.246	1.443
	−0.314	0.111	0.943	7.688
L2	0.707	−0.349	−0.615	1.446
	0.056	0.895	−0.443	0.729
	0.705	0.279	0.652	1.485
L3	0.538	0.784	0.310	5.476
	−0.810	0.583	−0.067	5.233
	−0.233	−0.215	0.948	23.311
L4	0.800	−0.440	−0.407	6.306
	0.440	0.892	−0.101	3.241
	0.407	−0.098	0.908	1.974

and isotropic. However, the librational motions of the small domain, loop and the terminal domain are of different magnitudes and directions, indicating anisotropic librational disorder and the prevalence of the librational motion in the rigid-body motion of the protein.

The magnitude of the librational motion of the loop (281–308) is about four times greater than that of the C-terminal domain (309–357) and the librational motion of the C-terminal domain is about three times greater than that of the small domain (2–99). The high-mobility loop bridges between two subdomains; the large domain (100–280) and the C-terminal domain (309–357). Contained within the less mobile large domain are residues Arg124, Arg126, Arg229, Cys271, Thr273 and Arg280 (that help to hold the substrates in place) and a catalytic residue, Glu225. The C-terminal domain includes catalytically important residues Arg309 and Glu314. The small domain (2–99) is also less mobile and includes residues Gly64, Val65, Gly66 and Tyr68, which help to hold the substrate arginine in place, and segment 61–65, which was proposed to be a specificity loop (Suzuki *et al.*, 1997; Zhou *et al.*, 1998). Thus, subdomains that have catalytically important residues exhibit the least mobility in the transition-state configuration.

In summary, the TLS analyses showed that transition-state structure of ariginine kinase consists of four rigid bodies. One domain is stationary, while libration is the prevalent mode of motion of the three other domains. Translation and screw-rotation motions are restricted. Thus, in addition to the previously characterized induced-fit closure of the active site (Forstner *et al.*, 1998; Zhou *et al.*, 2000) on each catalytic cycle, there is a reduction in the mobilities of the different rigid groups as the closed active form is stabilized in the transition state.

In conclusion, analysis at atomic resolution gives coordinates with precision of about 0.04 Å, sufficient now to confirm that the reactants are pre-aligned precisely. The precision is unexpectedly high (within 2.9° of the optimal attack configuration), suggesting that there has been evolutionary selection for substrate pre-alignment and that it is an important contributor to bimolecular catalysis. The capability, at high resolution, of refining atomic displacement factors shows that motion within the active site is frozen. Substrate *B* factors are lower than those of protein and most catalytic residues are contained within the least mobile enzyme rigid group. The high-resolution structure indicates the presence of a hydrogen bond between the β-phosphate and our analogue of the γ-phosphate, implying that the reaction is likely to proceed with a concerted proton transfer between β- and γ-phosphates as the P—N bond is formed/broken.

We thank Eliza Ruben for the p*K* calculation and gratefully acknowledge the funding of National Institute of Health for the project R01GM55837.

References

Bruice, T. C. & Benkovic, S. J. (2000). *Biochemistry*, **39**, 6267–6274.
Brünger, A. T. (1992). *Nature (London)*, **355**, 472–475.
Brünger, A. T., Adams, P. D., Clore, G. M., DeLano, W. L., Gros, P., Grosse-Kunstleve, R. W., Jiang, J. S., Kuszewski, J., Nilges, M., Pannu, N. S., Read, R. J., Rice, L. M., Simonson, T. & Warren, G. L. (1998). *Acta Cryst.* D**54**, 905–921.
Collaborative Computational Project, Number 4 (1994). *Acta Cryst.* D**50**, 760–763.
Dafforn, A. & Koshland, D. E. Jr (1971). *Proc. Natl Acad. Sci. USA*, **68**, 2463–2467.
Dauter, Z., Lamzin, V. S. & Wilson, K. S. (1997). *Curr. Opin. Struct. Biol.* **7**, 681–688.
Eder, M., Fritz-Wolf, K., Kabsch, W., Wallimann, T. & Schlattner, U. (2000). *Proteins*, **39**, 216–225.
Eder, M., Schlattner, U., Becker, A., Wallimann, T., Kabsch, W. & Fritz-Wolf, K. (1999). *Protein Sci.* **8**, 2258–2269.
Ellington, W. R. (2001). *Annu. Rev. Physiol.* **63**, 289–325.
Forstner, M., Manfred, K., Laggner, P. & Wallimann, T. (1998). *Biophys. J.* **75**, 1016–1023.
Fritz-Wolf, K., Schnyder, T., Wallimann, T. & Kabsch, W. (1996). *Nature (London)*, **381**, 341–345.
Hansen, D. E. & Knowles, J. R. (1981). *J. Biol. Chem.* **256**, 5967–5969.
Harata, K., Abe, Y. & Muraki, M. (1998). *Proteins*, **30**, 232–243.
Harata, K., Abe, Y. & Muraki, M. (1999). *J. Mol. Biol.* **287**, 347–358.
Harding, M. M. (1999). *Acta Cryst.* D**55**, 1432–1443.
Holbrook, S. R., Dickerson, R. E. & Kim, S. (1985). *Acta Cryst.* B**41**, 255–262.
Holbrook, S. R. & Kim, S. H. (1984). *J. Mol. Biol.* **173**, 361–388.
Howlin, B., Moss, D. S. & Harris, G. W. (1989). *Acta Cryst.* A**45**, 851–861.
Hutter, M. C. & Helms, V. (1999). *Protein Sci.* **8**, 2728–2733.
Hutter, M. C. & Helms, V. (2000). *Protein Sci.* **9**, 2225–2231.
Izzat, M. R. & Christensen James, J. (1970). *Handbook of Biochemistry*, edited by H. A. Sober, 2nd ed., p. J-66. Boca Raton, FL, USA: CRC Press.
Jones, T. A., Zou, J.-Y., Cowan, S. W. & Kjeldgaard, M. (1991). *Acta Cryst.* A**47**, 110–119.
Katz, A. K., Glusker, J. P., Beebe, S. A. & Bock, C. W. (1996). *J. Am. Chem. Soc.* **118**, 5752–5763.
Laskowski, R. A., MacArthur, M. W., Moss, D. S. & Thornton, J. M. (1993). *J. Appl. Cryst.* **26**, 283–291.
Lau, E. Y., Kahn, K., Bash, P. A. & Bruice, T. C. (2000). *Proc. Natl Acad. Sci. USA*, **97**, 9937–9942.
Lightstone, F. C. & Bruice, T. C. (1996). *J. Am. Chem. Soc.* **118**, 2595–2605.
Lightstone, F. C. & Bruice, T. C. (1998) *Bioorg. Chem.* **26**, 193–199.
Longhi, S., Czjzek, M. & Cambillau, C. (1998). *Curr. Opin. Struct. Biol.* **8**, 730–737.

Luzzati, V. (1952). *Acta Cryst.* **5**, 802–810.
McLaughlin, A. & Cohn, C. M. (1972). *J. Biol. Chem.* **247**, 4382–4388.
Merritt, E. A. (1999). *Acta Cryst.* D**55**, 1109–1117.
Mesecar, A. D., Stoddard, B. L. & Koshland, D. E. Jr (1997). *Science*, **277**, 202–206.
Milner-White, E. J. & Watts, D. C. (1971). *Biochem. J.* **122**, 727–740.
Otwinowski, Z. & Minor, W. (1997). *Methods Enzymol.* **276**, 307–326.
Page, M. I. & Jencks, W. P. (1971). *Proc. Natl Acad. Sci. USA*, **68**, 1678–1683.
Papiz, M. Z. & Prince, S. M. (1996). *Proceedings of the CCP4 Study Weekend. Macromolecular Refinement*, edited by E. Dodson, S. Moore & S. Bailey, pp. 115–123. Warrington: Daresbury Laboratory.
Ramakrishnan, C. & Ramachandran, G. N. (1965). *Biophys. J.* **5**, 909–933.
Rao, B. D. & Cohen, M. (1977). *J. Biol. Chem.* **252**, 3344–3350.
Rao, J. K., Bujacz, G. & Wlodawer, A. (1998). *FEBS Lett.* **439**, 133–137.
Rosenfield, R. E., Trueblood, K. N. & Dunitz, J. D. (1978). *Acta Cryst.* A**34**, 828–829.
Sali, A., Veerapandian, B., Cooper, J. B., Moss, D. S., Hofmann, T. & Blundell, T. L. (1992). *Proteins*, **12**, 158–170.
Schlattner, U., Forstner, M., Eder, M., Stachowiak, O., Fritz-Wolf, K. & Wallimann, T. (1998). *Mol. Cell. Biochem.* **184**, 125–140.
Schomaker, V. & Trueblood, K. N. (1968). *Acta Cryst.* B**24**, 63–76.
Sheldrick, G. M. (1990). *Acta Cryst.* A**46**, 467–473.
Sheldrick, G. M. & Schneider, T. R. (1997). *Methods Enzymol.* **277**, 319–343.
Shen, Y. Q., Tang, L., Zhou, H. M. & Lin, Z. J. (2001). *Acta Cryst.* D**57**, 1196–1200.
Stec, B., Zhou, R. & Teeter, M. (1995). *Acta Cryst.* D**51**, 663–681.
Suzuki, T., Kawasaki, Y., Furukohri, T. & Ellington, W. R. (1997). *Biochim. Biophys. Acta*, **1343**, 152–159.
Teixeira, S., Lo Leggio, L., Pickersgill, R. & Cardin, C. (2001). *Acta Cryst.* D**57**, 385–392.
Tisi, Y., Bax, B. & Loew, A. (2001). *Acta Cryst.* D**57**, 187–193.
Villa, J., Strajbl, M., Glennon, T. M., Sham, Y. Y., Chu, Z. T. & Warshel, A. (2000). *Proc. Natl Acad. Sci. USA*, **97**, 11899–11904.
Warshel, A. (1998). *J. Biol. Chem.* **273**, 27035–27038.
Wilson, M. A. & Brunger, A. T. (2000). *J. Mol. Biol.* **301**, 1237–1256.
Yang, A. S., Gunner, M. R., Sampogna, R., Sharp, K. & Honig, B. (1993). *Proteins*, **15**, 252–265.
Zhou, G., Ellington, W. R. & Chapman, M. S. (2000). *Biophys. J.* **78**, 1541–1550.
Zhou, G., Parthsarathy, G., Somasundaram, T., Ables, A., Roy, L., Strong, S. J., Ellington, W. R. & Chapman, M. S. (1997). *Protein. Sci.* **6**, 444–449.
Zhou, G., Somasundaram, T., Blanc, E., Parthsarathy, G., Ellington, W. R. & Chapman, M. S. (1998). *Proc. Natl Acad. Sci. USA*, **95**, 8449–8454.